Acta Cryst. (1960). **13**, 171

Electron Diffraction Study of Evaporated Carbon Films.*

By J. Kakinoki, K. Katada, T. Hanawa and T. Ino

The Institute of Polytechnics, Osaka City University, Osaka, Japan

(*Received* 14 *March* 1959 *and in revised form* 11 *August* 1959)

The structure of evaporated carbon films has been studied by electron diffraction using a camera with a rotating sector. Films of 100 Å thickness were used. Eleven halos were observed in the range of $s=(4\pi/\lambda)\sin\theta<33$ Å^{-1}. Both the radial distribution and the correlation methods were applied to the analysis of data.

Results obtained are as follows. Two kinds of bond distances exist in the film. One is the graphite-like 1·41 Å, and the other is the diamond-like 1·55 Å. The number of the diamond-like distances is somewhat larger than that of the graphite-like distances. Mean deviations of these equilibrium distances are $0{\cdot}11\sim0{\cdot}12$ Å, which are about twice as large as those found in free molecules. The atomic distribution around any atom becomes uniform beyond several Ångström units. The probable atomic arrangement in the film is a three-dimensional random network consisting of graphite-like and diamond-like configurations. A model of such atomic arrangement is proposed and compared with structures of other amorphous carbons.

Introduction

There are a few papers on thin films in amorphous state studied by electron diffraction. Some of them are, for example, those by Coumoulos (1943), Distler & Pinsker (1949, 1950), Kakinoki (1949) and Kakinoki, Murata & Katada (1949). However, only a few halos (3 or 4) were obtained by all of these authors except by us whereby 8 or more halos were obtained in the range of $s<20$ Å^{-1}. This difference seems to be mainly due to the fact that the films used by others were not so thin that outer halos were masked by the intense background caused by the multiple scattering of electrons. With a film thin enough to reduce the multiple scattering as in our case, many outer halos can be obtained just as in the case of free molecules. In the present paper, results of the study of evaporated thin films of carbon by electron diffraction will be dealt with.

Recently, thin films of carbon evaporated in vacuum are widely used in the field of electron microscopy as a replica or as a supporter of samples. This is partly because the film is mechanically very strong. As for its structure, however, it is only indicated that the film is in amorphous state because it gives a few halos by electron diffraction. Most of the X-ray studies of the so-called amorphous carbons showed that their structure was an aggregate of very small particles of graphite. As will be seen later, however, their X-ray diagrams are different from patterns obtained from evaporated carbon films by electrons. Hence, the electron-diffraction study of evaporated carbon films is very interesting.

* A preliminary work on this subject was read at the Fourth International Congress of I.U.Cr., July, 1957, in Montreal (*Acta Cryst.* (1957), **10**, 829).

Experimental

Thin films of carbon are prepared by the method of vacuum evaporation (Bradley, 1954). In a vacuum of 10^{-4} mm. Hg, films are formed at the rate of deposition of about 50 Å · sec.$^{-1}$ on the surfaces of glass plates, 20 cm. apart from locally heated carbon rods. The rod is of pure carbon for spectroscopic use. The film is floated on water surface and is scooped up on a specimen holder of brass, having several holes of 0·5 mm. diameter.*

The film thickness is measured by multiple-beam interferometry (Tolansky, 1948). Films of about 100 Å thickness are used.

The density of the specimen, necessary for analysis, is about 2·4 g.cm.$^{-3}$, which is determined from its thickness, area and weight (10^{-6} g.cm.$^{-2}$) measured by a quartz torsion balance. It is very difficult to determine the density with high accuracy since the specimen is very thin and light.

A camera with a rotating sector is used to obtain the diffraction patterns of the specimen under an accelerating voltage of 60 kV. The s^3- and s^2-sectors are used when the camera lengths are 12 cm. and 30 cm., respectively (Ino, 1953).

75% of the incident electrons can be detected after passing through the specimen by a Faraday cage with an aparture of 0·1 mm. diameter which is set at a distance of 10 cm. behind the specimen. This percentage is comparable with that obtained in the case of electron diffraction by free molecules (Karle & Karle, 1950*b*). Hence, the effect of multiple scattering of electrons may be considered to be not appreciable.

* The diameter of electron beam used was about 0·2 mm. at the position of the specimen.

Intensity data

Photographic plates, rapidly rotating about the center of the pattern, are radially microphotometered, and the photographic densities are converted into the intensities of electrons by the Karle–Karle method (Karle & Karle, 1949, 1950*a*).

The intensity is measured up to $s=27$ Å^{-1}, s being $(4\pi/\lambda).\sin\theta$, where λ is the wave-length of electrons and θ a half of the scattering angle. Nine halos can be found in this region. Moreover, two additional halos can be detected visually outside of $s=27$ Å^{-1}. It is remarkable that a distinct halo is found at such a small angle as $s=1{\cdot}2$ Å^{-1} and has a deep minimum inside of it. From this total intensity the structure sensitive intensity $I_m(s)$ is obtained as follows:

$$I_m(s)=C\left(\frac{\text{total intensity}}{\text{background intensity}}-1\right),$$

where C is a constant. The final $I_m(s)$ curve which is shown by the full line in Fig. 1 is obtained after successive approximations for choosing the best background intensity (Karle & Karle, 1950*a*). The dotted curve for $s>27$ Å^{-1} in Fig. 1 is a visual one. The s-values of maxima are listed in Table 1 together with those of ($hk0$) and ($00l$) reflections of graphite. The dotted part is not used in the radial distribution analysis but is used in the correlation method.

Table 1. *The s-values of maxima in $I_m(s)$ of the evaporated carbon film and of some ($hk0$) and ($00l$) reflections of graphite*

Evaporated carbon film		Graphite crystal	
No. of maximum	s-Value (Å^{-1})	(hkl)	s-Value (Å^{-1})
1	1·2	(002)	1·88
2	2·9	(100)	2·95
3	5·5	(110)	5·11
		(200)	5·90
4	8·6	(210)	7·82
		(300)	8·86
5	10·4	(220)	10·2
		(310)	10·6
6	13·5		
7	18·1		
8	22·4		
9	24·8		
10	28·5		
11	32		

As is well-known, the structure sensitive intensity $I_m(s)$ for a substance involving one kind of element is expressed as

$$I_m(s)=\frac{Z^2+Z}{Z^2}\cdot\frac{(Z-f(s))^2}{(Z-f(s))^2+S(s)}\times\int_0^\infty 4\pi r^2\{\varrho(r)-\varrho_0\}\frac{\sin sr}{sr}\,dr, \quad (1)$$

where Z, $f(s)$ and $S(s)$ are the atomic number, the atomic scattering factor and the incoherent intensity function for X-rays, respectively. $\varrho(r)$ is the radial atomic distribution function such that $4\pi r^2\varrho(r).dr$ is the number of atoms which lie at the distance between r and $r+dr$ from any given atom, and ϱ_0 is its average, that is, $\varrho_0=N/V=N_0d/M$, where N is the number of atoms in the effective volume V of the specimen for the scattering of electrons, N_0 Avogadro's number, d the density of the specimen and M the atomic weight.

If the reduced intensity $I(s)$ is put as

$$I(s)=\int_0^\infty 4\pi r^2\{\varrho(r)-\varrho_0\}\frac{\sin sr}{sr}\,dr, \quad (2)$$

it can be obtained from the experimental $I_m(s)$ as follows:

$$I(s)=M(s).I_m(s),$$
$$M(s)=I(s)/I_m(s)=\frac{Z}{Z+1}\left\{1+\frac{S(s)}{(Z-f(s))^2}\right\}.$$

The curves of $I(s)$ and $M(s)$ are shown in Fig. 1. $M(s)$ is found to have large values in the region of small s and to approach to unity with increase of s-value.* Therefore, $M(s)$ has such an effect as to emphasize the amplitudes of $I_m(s)$ in the region of small s.

The influence of the difference in the conditions of evaporation upon the diffraction pattern is examined. Some films are prepared under lower vacuum ($10^{-2}\sim10^{-3}$ mm. Hg), and some on a cleavage surface of crystals such as rock salt, but no difference is visually detected among the diffraction patterns. It is also confirmed that films evaporated from two kinds of carbon rods do not show any difference between their patterns, while the rods are found to give different X-ray powder diagrams from each other.

Radial distribution analysis

Applying the Fourier inversion on equation (2), the radial atomic distribution function is given as follows:

$$\left.\begin{aligned}&4\pi r\Delta(r)=4\pi r\{\varrho(r)-\varrho_0\}=\frac{2}{\pi}\int_0^\infty sI(s)\sin sr\,ds,\\ &\text{or}\\ &4\pi r^2\varrho(r)=4\pi r^2\varrho_0+\frac{2}{\pi}r\int_0^\infty sI(s)\sin sr\,ds.\end{aligned}\right\} \quad (3)$$

In order to diminish the termination effect, a damping factor $\exp(-as^2)$ is multiplied as usual, that is,

$$4\pi r\Delta^*(r)=\frac{2}{\pi}\int_0^\infty sI(s)\exp(-as^2)\sin sr\,ds$$
$$\fallingdotseq\frac{2}{\pi}\int_0^{s_0} sI(s)\exp(-as^2)\sin sr\,ds,$$

* Numerical values of $f(s)$ are taken from the table by Viervoll & Øgrim (1949). Those of $S(s)$ are taken from the text-book of Compton & Allison (1935) and extrapolated to larger s.

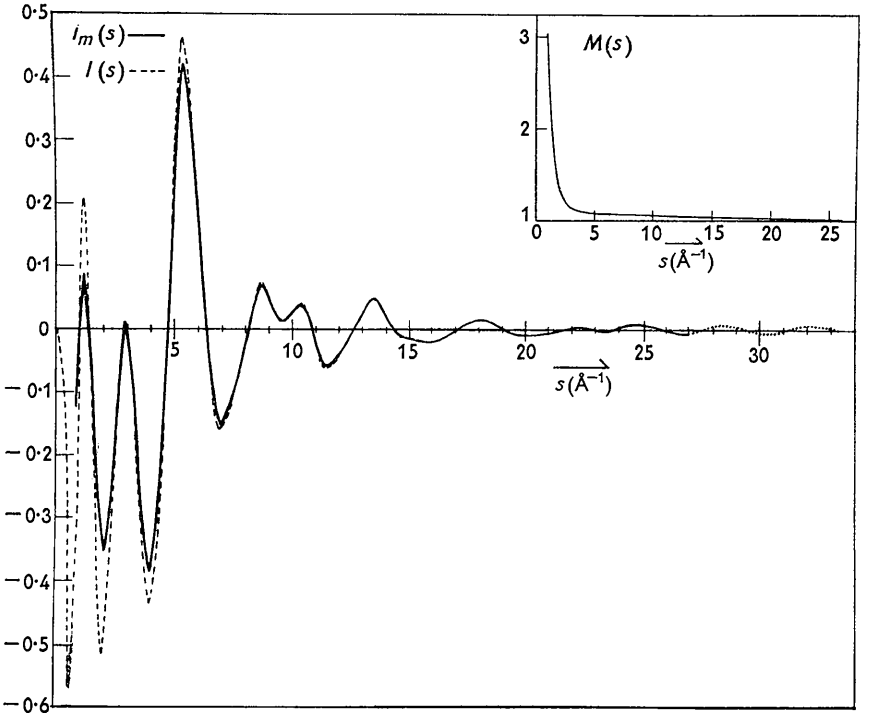

Fig. 1. Experimental intensity curves of $I_m(s)$ (full line) and $I(s)$ (broken line). Dotted line shows a visually estimated part. The curve of $M(s)$ is also shown.

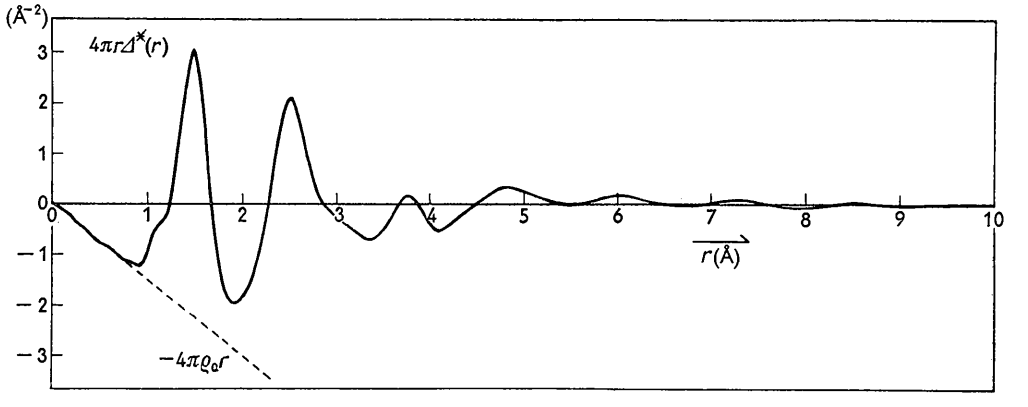

Fig. 2. The curve of $4\pi r\Delta^*(r)$.

where s_0 is the observable upper limit of s. Now, $4\pi r\Delta^*(r)$ differs from $4\pi r\Delta(r)$, but $4\pi r\varrho_0$ can be shown to be unmodified by the factor $\exp(-as^2)$, so that

$$4\pi r\varrho^*(r) = 4\pi r\varrho_0 + \frac{2}{\pi}\int_0^{s_0} sI(s)\exp(-as^2)\sin sr\,ds\,. \quad (4)$$

The intensity $I(s)$ in the range of $s<27$ Å^{-1} is used in computation of the integral in equation (4). The arbitrary constant a is chosen to be equal to $0{\cdot}3\times10^{-2}$ Å^2, so that $\exp(-as^2)=0{\cdot}1$. The integral is replaced by the sum of 85 terms of the integrand spaced at equal intervals of $\Delta s=\pi/10$ Å^{-1}. This approximation yields no practical error in the result in the range of $0\leqq r<10$ Å, if $4\pi r\Delta^*(r)$ is almost zero beyond $r=10$ Å (Franklin, 1950; Ino, 1957). The summation is carried out by means of the punched-card system.

The obtained curve of $4\pi r\Delta^*(r)$ illustrated in Fig. 2 shows that $4\pi r\Delta^*(r)$ converges rapidly to zero. Therefore, it is reasonable to assume that $4\pi r\Delta^*(r)$ vanishes practically beyond $r=10$ Å. The curve of $4\pi r^2\varrho^*(r)$ is shown in Fig. 3 (full line).

The analysis of this curve is carried out as follows. As will be suggested from the correlation method, the first peak at $r=1{\cdot}50$ Å on the curve of $4\pi r^2\varrho^*(r)$ is reasonably decomposed into two peaks, so that the first peak can be expressed by

$$4\pi r^2\varrho^*(r) = A_{1g}\{4\pi(a+b_{1g})\}^{-\frac{1}{2}} \exp\left[-(r-r_{1g})^2/4(a+b_{1g})\right] + A_{1d}\{4\pi(a+b_{1d})\}^{-\frac{1}{2}} \exp\left[-(r-r_{1d})^2/4(a+b_{1d})\right], \quad (5)$$

if each component has the Gaussian form. In this expression a is the constant in $\exp(-as^2)$ and $2b_{1g}$ and $2b_{1d}$ are the mean square deviations of two distances r_{1g} and r_{1d}, respectively (Karle & Karle, 1949, 1950*a*). A_{1g} and A_{1d} are the numbers per atom of distances r_{1g} and r_{1d}, respectively, and hence $A_{1g}+A_{1d}$ gives the mean co-ordination number around a carbon atom. The most probable values of parameters are found to be

$r_{1g}=1{\cdot}41\sim1{\cdot}42$ Å $r_{1d}=1{\cdot}55\sim1{\cdot}56$ Å
$b_{1g}=0{\cdot}6\sim0{\cdot}7\times10^{-2}$ Å^2 $b_{1d}=b_{1g}$
$A_{1g}=1{\cdot}4\sim1{\cdot}5$ $A_{1d}=1{\cdot}7$
$(A_{1d}/A_{1g}=1{\cdot}1\sim1{\cdot}2)$.

The individual peaks with these values are shown in Fig. 3 (broken lines). The distances r_{1g} and r_{1d} correspond to the graphite-like and the diamond-like bond distances, respectively, and mean deviations of these distances, $(2b_{1g})^{\frac{1}{2}}$ and $(2b_{1d})^{\frac{1}{2}}$, are deduced to be $0{\cdot}11\sim0{\cdot}12$ Å.

The analysis of the second peak is more or less arbitrary. However, considering the second and the third neighbors in the graphite-like and the diamond-like atomic configurations, this peak can be decomposed as shown in Fig. 3 (broken lines) and the following results are obtained.

$r_{2g}=2{\cdot}45$ Å, $b_{2g}=2{\cdot}0\times10^{-2}$ Å^2, $A_{2g}=2{\cdot}8$,
$r_{2d}=2{\cdot}54$ Å, $b_{2d}=b_{2g}$, $A_{2d}=5{\cdot}0$,

and

$r_{3g}=2{\cdot}83$ Å, $b_{3g}=3{\cdot}5\times10^{-2}$ Å^2, $A_{3g}=1{\cdot}0$,
$r_{3d}=2{\cdot}98$ Å, $b_{3d}=b_{3g}$, $A_{3d}=3{\cdot}5$.

After subtracting the Gaussian components of the first and the second neighbor distances from the experimental $4\pi r^2\varrho^*(r)$, there remain some surplus portions at $r=1{\cdot}1$ Å and $1{\cdot}9$ Å as shown in Fig. 3 (hatched portions). It cannot be decided with confidence whether these parts are due to errors or to contributions of other distances such as C≡C.

Calculation of intensities (correlation method)

The behavior of the intensity curve except the innermost halo can be well represented by the contribution of shorter distances alone (Kakinoki, 1949). Along this line the intensity calculation is first performed by

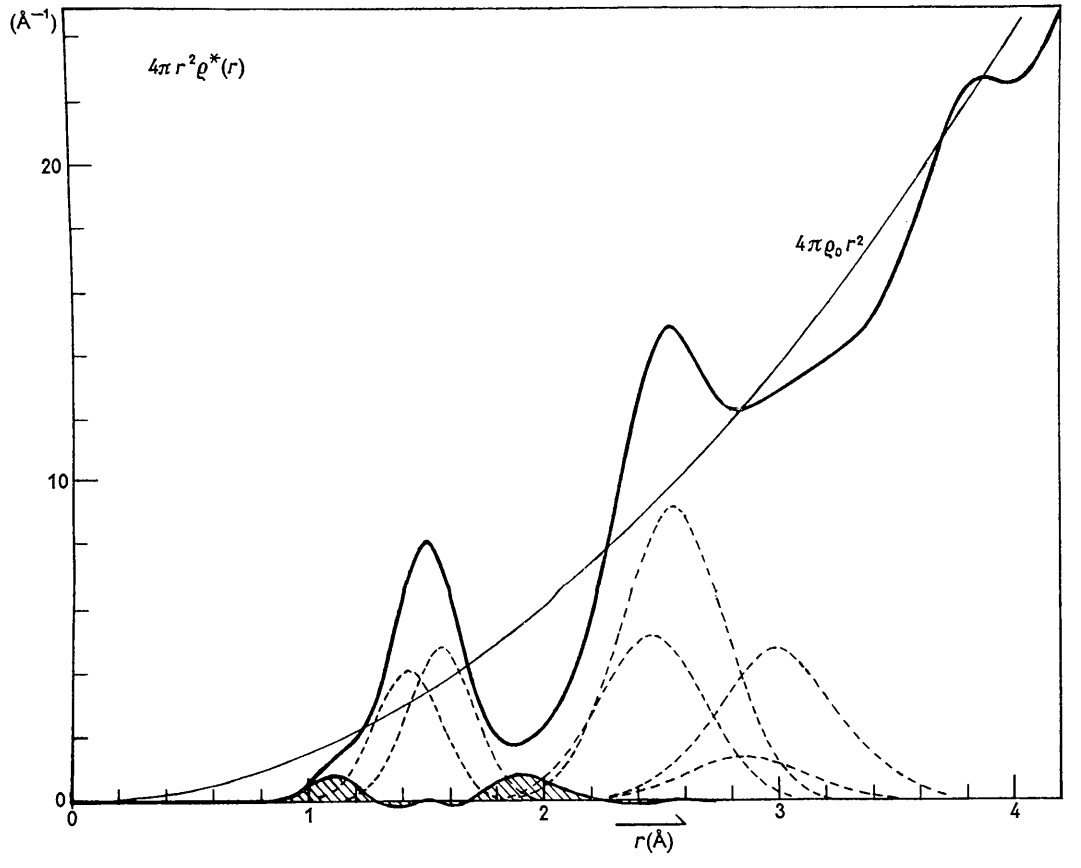

Fig. 3. Full line: the experimental curve of $4\pi r^2\varrho^*(r)$. Broken lines: the components in Gaussian form with the most probable values of parameters. Hatched portions: the remainder after subtracting the above components from $4\pi r^2\varrho^*(r)$.

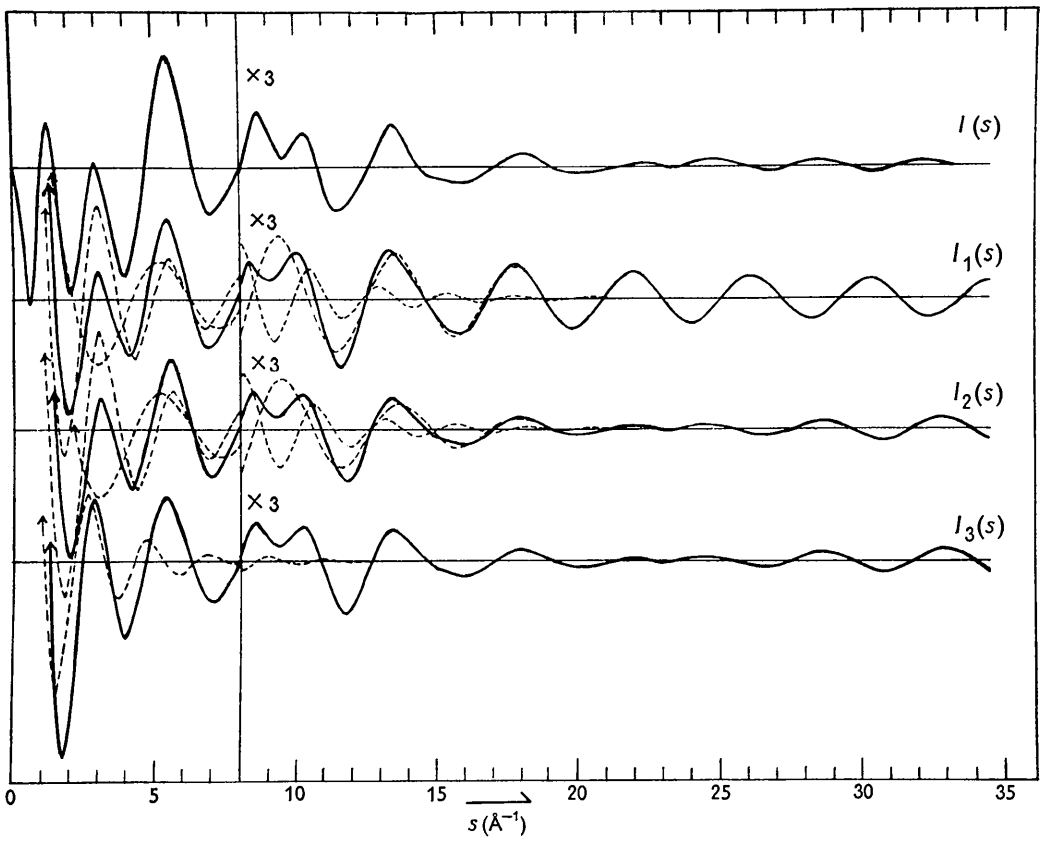

Fig. 4. Comparison between the observed and the calculated intensities $I(s)$, $I_1(s)$, $I_2(s)$ and $I_3(s)$. Broken lines in $I_1(s)$ and $I_2(s)$ show the first and the second neighbor contributions. Broken line in $I_3(s)$ shows the third neighbor contribution. The ordinates are multiplied by three beyond $s=8$ Å^{-1}.

$$I_1(s)=\frac{\sin 1{\cdot}50s}{1{\cdot}50s}+2{\cdot}5\exp\left(-1{\cdot}3\times10^{-2}s^2\right)\frac{\sin 2{\cdot}54s}{2{\cdot}54s}\,.$$

where the numerical values are determined by crude estimation of the first and the second peaks of $4\pi r^2\varrho^*(r)$. In Fig. 4 the curve of $I_1(s)$ is shown together with the observed $I(s)$ curve. It is interesting to see that the maxima and minima of the observed intensity are satisfactorily reproduced up to $s=20$ Å^{-1}, and that the second term of $I_1(s)$ has no appreciable contribution to the curve in the region of larger s.

A very important fact is that the curve of $I_1(s)$ shifts in phase from that of $I(s)$ beyond $s=24$ Å^{-1}. This suggests that there should be two or more kinds of bond distances instead of a single kind of 1·50 Å. Thus, it is reasonable to adopt the graphite-like bond distance r_{1g} and the diamond-like r_{1d}. All combinations of $r_{1g}=1{\cdot}40$, 1·41, 1·42, 1·43 Å, $r_{1d}=1{\cdot}53$, 1·54, 1·55, 1·56 Å and $A_{1d}/A_{1g}=0{\cdot}8$, 0·9, 1·0, 1·1, 1·2, 1·3 are considered. The curves for some of these combinations are shown in Fig. 5 together with $I(s)$. The best combination is found to be

$$r_{1g}=1{\cdot}41\text{ Å},\quad r_{1d}=1{\cdot}55\text{ Å},\quad A_{1d}/A_{1g}=1{\cdot}0\sim1{\cdot}1\,.$$

For simplicity, the calculated intensities have so far been compared with the observed one in a limited range of $s>20$ Å^{-1}. In order to ascertain the above parameters to be acceptable in the whole range of s except in the neighborhood of the innermost maximum, the following intensity is calculated.

$$I_2(s)=\frac{1}{2{\cdot}1}\left[1{\cdot}0\frac{\sin 1{\cdot}41s}{1{\cdot}41s}+1{\cdot}1\frac{\sin 1{\cdot}55s}{1{\cdot}55s}+\exp\left(-1{\cdot}3\times10^{-2}s^2\right)\times\left\{2\times1{\cdot}0\frac{\sin 2{\cdot}44s}{2{\cdot}44s}+3\times1{\cdot}1\frac{\sin 2{\cdot}53s}{2{\cdot}53s}\right\}\right].$$

This expression contains not only the two kinds of the first neighbor distances but also those of the second neighbor distances both in graphite-like and diamond-like configurations with the value of $b_{2g}-b_{1g}=b_{2d}-b_{1d}=1{\cdot}3\times10^{-2}$ Å^2 obtained from the radial distribution analysis. The first factor (1/2·1) is introduced for normalization of both intensities $I_1(s)$ and $I_2(s)$. The curve of $I_2(s)$ given in Fig. 4 is in good agreement with the observed $I(s)$ curve even in the range of $s<20$ Å^{-1} and the second neighbor contributions are found to be negligible in the range of $s>20$ Å^{-1}.

It is also confirmed that the third neighbor dis-

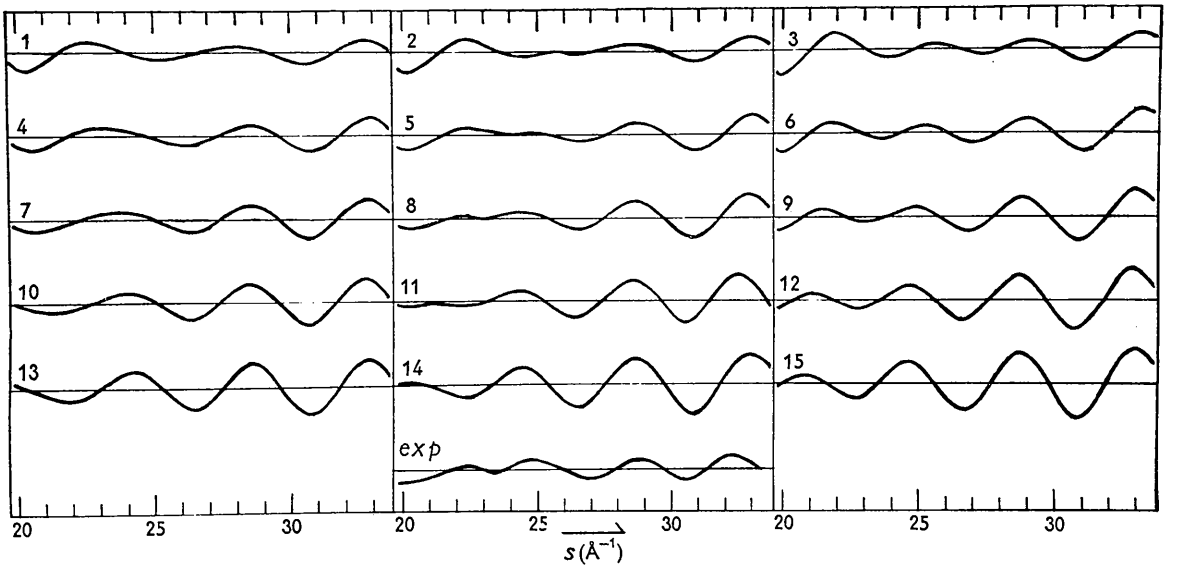

Fig. 5. Comparison between the observed and the calculated intensities. The fifteen calculated intensities,

$$\frac{\sin sr_{1g}}{sr_{1g}} + \frac{A_{1d}}{A_{1g}} \cdot \frac{\sin sr_{1d}}{sr_{1d}}$$

have the following values of parameters.

r_{1g} (Å)	r_{1d} (Å)	A_{1d}/A_{1g} = 0·8	A_{1d}/A_{1g} = 1·0	A_{1d}/A_{1g} = 1·3
1·42	1·54	Curve 1	Curve 2	Curve 3
1·41	1·54	4	5	6
1·41	1·55	7	8	9
1·41	1·56	10	11	12
1·40	1·56	13	14	15

tances have no important contribution to the intensity curve. An example is

$$I_3(s) = I_2(s) + \frac{1}{2{\cdot}1} \exp\left(-2{\cdot}8 \times 10^{-2} s^2\right) \times \left\{1 \times 1{\cdot}0 \frac{\sin 2{\cdot}83s}{2{\cdot}83s} + 3 \times 1{\cdot}1 \frac{\sin 2{\cdot}98s}{2{\cdot}98s}\right\},$$

which is shown in Fig. 4. Moreover, there may be other kinds of distances, for example, $r = 1{\cdot}1$ Å corresponding to the surplus peak of the radial distribution curve (Fig. 3) and $r = 1{\cdot}5$ Å which may be found between a graphite-like atom and a diamond-like atom.* The contribution of $r = 1{\cdot}1$ Å to the intensity curve is negligible because its abundance is very small. The contribution of $r = 1{\cdot}5$ Å to the intensity curve, however, should be of great significance if its abundance is large, as was already seen on the curve $I_1(s)$ in Fig. 4. But it is confirmed that it does not change the feature of the intensity curve so far as the ratio of its abundance to $A_{1g} + A_{1d}$ is smaller than $\frac{1}{5}$.

* Although the value of 1·5 Å is accidentally in coincidence with that of the first peak on the radial distribution curve, the same value may be found between a pair of C-atoms one of which is at a corner of the graphite hexagon and the other at an end of the diamond configuration, just as C–(CH_3) in ⬡C–(CH_3) (toluene).

Discussion

Method

The electron-diffraction diagram of the evaporated carbon film is a typical halo-pattern like that of free molecules. Therefore, the method of analysis used here is similar to that for free molecules. There are, however, some different points between them.

The first point is that the measurement of the density of the specimen is necessary in the present case for obtaining the complete radial distribution function $4\pi r^2 \varrho(r)$. Since the density of thin films is difficult to measure, its uncertainty may be one of the sources of error. The second point is that it is difficult to estimate the value of r_0 beyond which $4\pi r \Delta^*(r)$ is practically zero, the interval Δs being given by $\Delta s \leqq \pi / r_0$. The third point is that it is impossible to obtain a complete set of distances for all atomic pairs necessary for calculation of the intensity.

Both correlation and radial distribution methods of analysis in which the three points mentioned above are considered are found to be powerful. It is the correlation method that gives the information that the first

peak on the radial distribution curve does not correspond to a single distance of 1·50 Å, but is comprised of two kinds of distances, 1·41 Å and 1·55 Å. The difference between these values and the ratio of their abundances are particularly sensitive to the behavior of the intensity in the region of large s. By the radial distribution method the abundances and the mean square deviations of these distances can be easily determined for the first neighbors. Thus, complete results can be successfully obtained by the co-operation of both methods.

It is interesting to note that, in the present case, the behavior of the observed intensity in the range of $s>20$ Å^{-1} is well reproduced by the first neighbor distances alone, while in the range of $2<s<20$ Å^{-1} the behavior of the observed intensity is reproduced mainly by the first and the second neighbor distances. The longer distances are responsible mainly for the existence of the distinct first halo at $s=1·2$ Å^{-1}, as in the case of polystyrene film whose corresponding halo is explained by the integral term including longer distances (Kakinoki, 1949).

Comparison with X-rays

There are more studies on amorphous materials by X-rays than those by electrons. The method of electron diffraction, however, is superior to X-rays in studying the short-range structure, because the diffraction intensity in the region of large s can be observed by electrons and this is very sensitive to short interatomic distances. Moreover, there are some possibilities of leading to some unreal structure unless the intensity data in the region of large s are used. For example, as seen from Fig. 4, if no intensity data is known beyond $s=18$ Å^{-1} which is the largest value of s observed by the Mo $K\alpha$ radiation ($\lambda=0·71$ Å),* it cannot be easily decided whether the direct C–C distance is of a single kind of 1·50 Å or of two kinds of 1·41 Å and 1·55 Å. The observation over a wide range is also advantageous for the radial distribution analysis.

Contribution from the highly disordered state of carbon

Franklin, in her paper on the interpretation of diffuse X-ray diagrams of carbon prepared by pyrolysis of polyvinylidene chloride, stated that $\frac{2}{3}$ of the whole carbon atoms were in the form of graphite-like layers and $\frac{1}{3}$ were in a highly disordered state (Franklin, 1950). She analyzed carefully the data both by the radial distribution and the correlation methods.

In her radial distribution method, however, the contribution of atomic pairs in the highly disordered state is not considered. Since a certain type of chemical bonds should be formed among carbon atoms even in such a state, these atomic pairs must contribute to the radial distribution curve as a peak at $r=1·4\sim1·5$ Å whose area is $\frac{1}{3}$ of the total area under the first peak. Hence, this contribution should not be neglected. It is also the case for the second peak. In her correlation method the contribution from the $\frac{1}{3}$ part to intensity is considered as indistinguishable from the independent scattering. This is not rigorous, but it may be permissible because the intensity maxima from the random layer structure of graphite are much stronger than those from the highly disordered structure.

Structure of the evaporated carbon film

From the analysis mentioned above, following model may be deduced regarding the structure of the film.

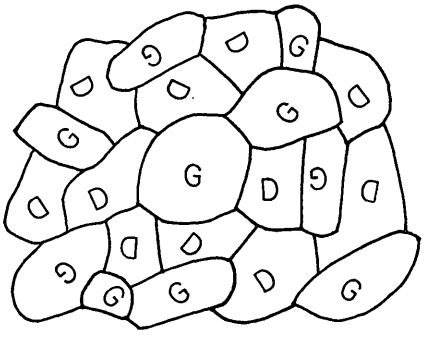

Fig. 6. Two-dimensional representation of arrangement of the graphite-like and the diamond-like regions.

Since two kinds of bonds are found, one may expect that there are two kinds of regions in the film, namely the graphite-like configuration (say, G-region) and the diamond-like one (say, D-region) as shown in Fig. 6, where, for simplicity, two-dimensional model is shown. The individual G- and D-regions should be as small as several Ångström units and have no mutual orientation because, as seen from Fig. 2, the radial distribution function approaches rapidly to its average.

These regions come into an assembly which should be so large as to produce a deep minimum inside of the innermost halo.* If such large particles (assemblies) are distributed separately as carbon flakes are in carbon black, the individual particles can be observed under an electron microscope. But an electron microscope observation of the film cannot reveal any discontinuity, hence such an assembly is considered to be the film itself.

A probable model of the atomic arrangement in the film is proposed in Fig. 7 together with models of graphite and diamond crystals. Such an atomic arrangement is a three-dimensional random network similar to that of glass. This model is consistent with the observed density of the film which is between those of graphite and diamond crystals, and it is responsible for the high mechanical strength of the film.

* Because of the damping nature of the atomic scattering factor for X-rays any halo is hardly detected in the region of large angle.

* Such a deep minimum as well as the innermost halo cannot be observed on the diffraction pattern from free molecules.

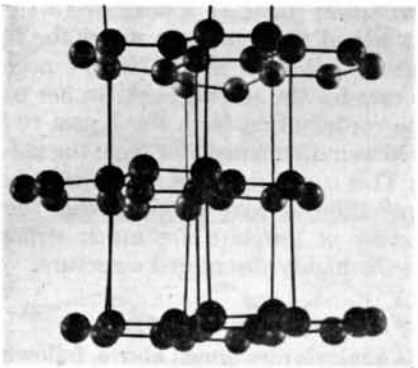

(*a*)

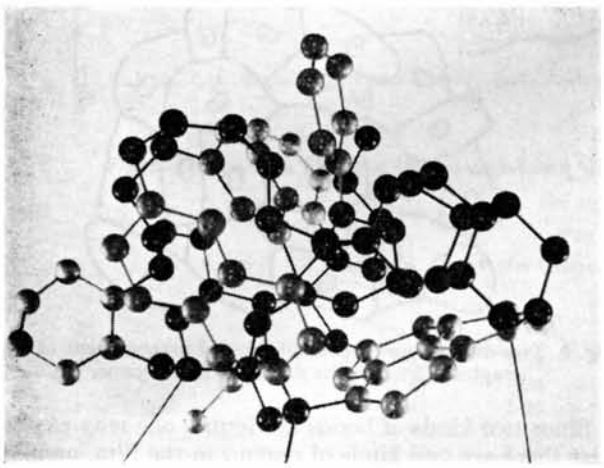

(*b*)

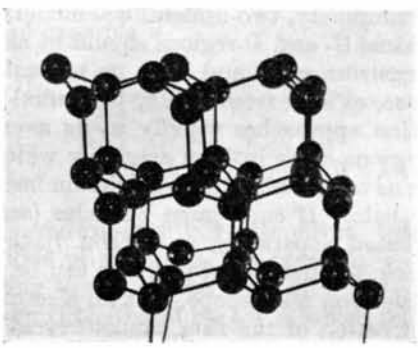

(*c*)

Fig. 7. Models of the atomic arrangements in the graphite crystal (*a*), in the evaporated carbon film (*b*) and in the diamond crystal (*c*). In (*b*), grey and black spheres represent the graphite-like and the diamond-like atoms, respectively.

There is some stress near the bonds by which the individual regions are connected with each other. Some fluctuation due to the stress can be expected in the interatomic distances of such bonds. This may well explain the observed large values of mean deviations, $(2b_{1g})^{\frac{1}{2}} = (2b_{1d})^{\frac{1}{2}} = 0{\cdot}11 \sim 0{\cdot}12$ Å, which are about twice as large as the usual values found in free molecules.

The ratio $A_{1d}/A_{1g} = 1{\cdot}1$ obtained from both methods of analysis indicates that diamond-like bonds exist in excess a little more than graphite-like bonds, while the number of diamond-like atoms may be a little less than that of graphite-like atoms if they are assumed to be given by $A_{1d}/4$ and $A_{1g}/3$, respectively. Comparing the observed ratios $A_{2g}/A_{1g} = 2$ and $A_{3g}/A_{1g} = 0{\cdot}7$ with the corresponding values of 2 and 1 in an infinite layer of graphite, it can be supposed that graphitic layers in the film are sufficiently small for the number of atoms of the third neighbor to be reduced appreciably. The situation is quite similar in the diamond-like region.

Amorphous carbons

A great variety of structures has been found in the so-called amorphous carbons by X-ray studies. These various structures depend strongly on the starting materials and the procedures by which the specimen is prepared. Attention has been paid in all of the studies mainly to the size and the degree of perfectness of graphite crystallites. Some examples are given by Warren (1934) and Franklin (1950). The size of graphite crystallites is much larger in Warren's sample than in Franklin's as deduced from the depth of the innermost minimum. Moreover, the random layer structure of graphite is verified to exist in Franklin's sample from the asymmetric feature of intensity maxima.

It is very interesting to know that large amount of the diamond-like distances exists in the evaporated film. Moreover, the structure of the film is a three-dimensional network involving the graphite-like and the diamond-like configurations, while that of the so-called amorphous carbons is only an aggregate of graphitic layers or graphite crystallites. Such a difference between structures is caused by the procedures of preparation. In the case of the vacuum evaporation the carbon film is formed by the recombination of atoms, molecules (C_2, C_3, ...) and ions. Hence, the structure of evaporated films does not depend on the starting materials.

There is a possibility for the highly disordered state proposed by Franklin to have such a structure as presented here.

Thus, the term 'amorphous' carbon is ambiguous and does not indicate a definite structure.

Further studies on the influence of conditions of evaporation such as evaporating speed and temperature of substrates, and on ageing effect, heat treatment and electrical properties of the film are very interesting. Experiments will be continued along this line.

It is our pleasure to express our sincere thanks to Prof. R. Uyeda and Mr H. Morimoto of Nagoya University for making available to us a set of microphotometer with a high speed rotating accessory. We also wish to thank Dr Y. Ueda of the Tokai-

Denkyoku Co. for supplying us with carbon rods. The present study is supported in part by the Scientific Research Grant from the Ministry of Education.

References

BRADLEY, D. E. (1954). *Brit. J. Appl. Phys.* **5**, 65.

COMPTON, A. H. & ALLISON, S. K. (1935). *X-rays in Theory and Experiment.* New York: D. Van Nostrand.

COUMOULOS, G. D. (1943). *Proc. Roy. Soc. Lond.* A, **182**, 166.

DISTLER, G. I. & PINSKER, Z. G. (1949). *Ž. Fiz. Khim. SSSR.* **23**, 1281.

DISTLER, G. I. & PINSKER, Z. G. (1950). *Ž. Fiz. Khim. SSSR.* **24**, 1152.

FRANKLIN, R. E. (1950). *Acta Cryst.* **3**, 107.

INO, T. (1953). *J. Phys. Soc. Jap.* **8**, 92.

INO, T. (1957). *J. Phys. Soc. Jap.* **12**, 495.

KAKINOKI, J. (1949). Scientific Papers from the Osaka Univ. No. 16.

KAKINOKI, J., MURATA, H. & KATADA, K. (1949). Scientific Papers from the Osaka Univ. No. 17.

KARLE, I. L. & KARLE, J. (1949). *J. Chem. Phys.* **17**, 1052.

KARLE, J. & KARLE, I. L. (1950*a*). *J. Chem. Phys.* **18**, 957.

KARLE, I. L. & KARLE, J. (1950*b*). *J. Chem. Phys.* **18**, 963.

TOLANSKY, S. (1948). *Multiple-Beam Interferometry of Surfaces and Films.* London: Oxford Univ. Press.

VIERVOLL, H. & ØGRIM, O. (1949). *Acta Cryst.* **2**, 277.

WARREN, B. E. (1934). *J. Chem. Phys.* **2**, 551.

Acta Cryst. (1960). **13**, 179

New Synthetic Garnets

BY S. GELLER AND C. E. MILLER WITH AN APPENDIX BY R. G. TREUTING

Bell Telephone Laboratories, Incorporated, Murray Hill, New Jersey, U.S.A.

(*Received* 14 *May* 1959 *and in revised form* 25 *June* 1959)

Twenty-three new synthetic garnets of types:

$$M^{2+}R_2^{3+}Mn_2Ge_3O_{12},\ M^{2+}R_2^{3+}M_2^{2+}Ge_3O_{12},\ R_3^{3+}M_2^{2+}GaGe_2O_{12} \text{ and } Ca_3M^{4+}M^{2+}Ge_3O_{12}$$

are reported. In these formulae, M^{4+} is a tetravalent metal ion of Zr, Sn or Ti; R^{3+} is an yttrium or gadolinium ion; M^{2+} is one of a variety of divalent metal ions, not all of which go into all the types. It is probable that R^{3+} could be almost any trivalent rare earth ion. Three other garnets are reported: $Mn_3NbZnFeGe_2O_{12}$; one of probable formula $Ca_3ZrFeGe_{2.8}O_{12}$, in which Fe has an average valence of 2·9 and $Y_2Mn_2FeGe_{2.8}O_{12}$ in which Fe has an average valence of 2·8. The latter two are defect structures. It is shown quantitatively that two-thirds of the Co^{2+} ions in $CoGd_2Co_2Ge_3O_{12}$ and in $CoY_2Co_2Ge_3O_{12}$ occupy octahedral positions, the remaining third occupying the dodecahedral positions. The distributions of ions in the other new garnets is discussed. To date, the Co^{2+} ion is the only one with non-spherical electronic configuration which is definitely known to occupy octahedral positions in the garnets. There are still no known garnets in which ions with non-spherical electronic configuration occupy tetrahedral positions.

The programming of the calculation of powder intensities including both real and imaginary parts of the dispersion corrections on the IBM 704 computer is briefly described in an appendix.

Introduction

The garnet structure belongs to space group O_h^{10}–$Ia3d$ with metal ions in 16*a*, 24*c* and 24*d* and oxygen (or fluorine) ions in 96*h*. It is convenient to write the chemical formula of one unit (see Gilleo & Geller, 1958*a*) $\{A_3\}[B_2](C_3)O_{12}$, where { } represent a *c* or dodecahedral site, [ ] an *a* or octahedral site and ( ) a *d* or tetrahedral site. The three sites are accessible to both magnetic and non-magnetic ions of a great variety, but conditions of electronic configuration and size determine the extent to which ions go into the different sites.

Yttrium–iron garnet, $\{Y_3\}[Fe_2](Fe_3)O_{12}$, has been studied very thoroughly and from various points of view. An accurate structure determination (Geller & Gilleo, 1957*a*) shows that the geometry of the $[Fe^{3+}]$–O–(Fe^{3+}) linkages is conducive to the strong magnetic interaction which is observed (Aleonard, Barbier & Pauthenet, 1956; Geller & Gilleo, 1957*b*). The results of the structure determination indicated also that if a magnetic rare earth ion were substituted for Y^{3+}, the magnetic interaction between it and a magnetic ion in a tetrahedral site would be stronger than that with a like magnetic ion in an octahedral site. Until recently no *direct c–a* or *c–d* interactions had been observed. Some of the compounds reported herein, having magnetic ions in *c* and *a* sites only, have been shown to have antiferromagnetic ordering with a resultant spontaneous magnetization at very